

Reliable Object Tracking by Multimodal Hybrid Feature Extraction and Transformer-Based Fusion

Hongze Sun^a, Rui Liu^a, Wuque Cai^a, Jun Wang^a, Yue Wang^a, Huajin Tang^b, Yan Cui^{a,c}, Dezhong Yao^{a,d,*}, and Daqing Guo^{a,*}

^aClinical Hospital of Chengdu Brain Science Institute, MOE Key Lab for NeuroInformation, School of Life Science and Technology, University of Electronic Science and Technology of China, Chengdu 611731, China.

^bCollege of Computer Science and Technology, Zhejiang University, Hangzhou 310027, China.

^cSichuan Academy of Medical Sciences and Sichuan Provincial People's Hospital, Chengdu 611731, China.

^dResearch Unit of NeuroInformation (2019RU035), Chinese Academy of Medical Sciences, Chengdu 611731, China.

Abstract

Visual object tracking, which is primarily based on visible light image sequences, encounters numerous challenges in complicated scenarios, such as low light conditions, high dynamic ranges, and background clutter. To address these challenges, incorporating the advantages of multiple visual modalities is a promising solution for achieving reliable object tracking. However, the existing approaches usually integrate multimodal inputs through adaptive local feature interactions, which cannot leverage the full potential of visual cues, thus resulting in insufficient feature modeling. In this study, we propose a novel multimodal hybrid tracker (MMHT) that utilizes frame-event-based data for reliable single object tracking. The MMHT model employs a hybrid backbone consisting of an artificial neural network (ANN) and a spiking neural network (SNN) to extract dominant features from different visual modalities and then uses a unified encoder to align the features across different domains. Moreover, we propose an enhanced transformer-based module to fuse multimodal features using attention mechanisms. With these methods, the MMHT model can effectively construct a multiscale and multidimensional visual feature space and achieve discriminative feature modeling. Extensive experiments demonstrate that the MMHT model exhibits competitive performance in comparison with that of other state-of-the-art methods. Overall, our results highlight the effectiveness of the MMHT model in terms of addressing the challenges faced in visual object tracking tasks.

Keywords: Object tracking, Multimodal fusion, Spiking neural networks, Transformer.

1. Introduction

Visual object tracking is a fundamental yet challenging computer vision task that has a wide range of applications in the real world [24, 25]. Benefiting from the progress achieved with respect to deep neural networks and big data, trackers based on feature modeling and end-to-end training have become the mainstream models for solving single object tracking problems [6, 1]. To address challenging visual scenes, researchers have recently proposed introducing more task-oriented visual cues by integrating multimodal information (such as thermal, depth and event information), thereby enhancing the robustness of feature modeling [42, 57, 16, 54].

Among these visual information modalities, event data recorded by bioinspired event cameras are attracting increasing attention [52, 28, 51].

In contrast with conventional frame-based cameras that employ light intensity to construct spatial appearance information, event cameras record light intensity changes in the temporal domain (as shown in Fig. 1), enabling the representation of sparse spatiotemporal information [5]. Due to their higher dynamic ranges and sampling frequencies, event cameras demonstrate inherent proficiency in challenging conditions, including environments with low light, scenes with high dynamic ranges, spatiotemporal coupling scenarios, and active filtering tasks [22]. In recent years, numerous event-based datasets have been published and utilized for various visual tasks, such as classification, recognition, optical flow estimation, object tracking and se-

*Corresponding authors: dyao@uestc.edu.cn (Dezhong Yao) and dqguo@uestc.edu.cn (Daqing Guo).

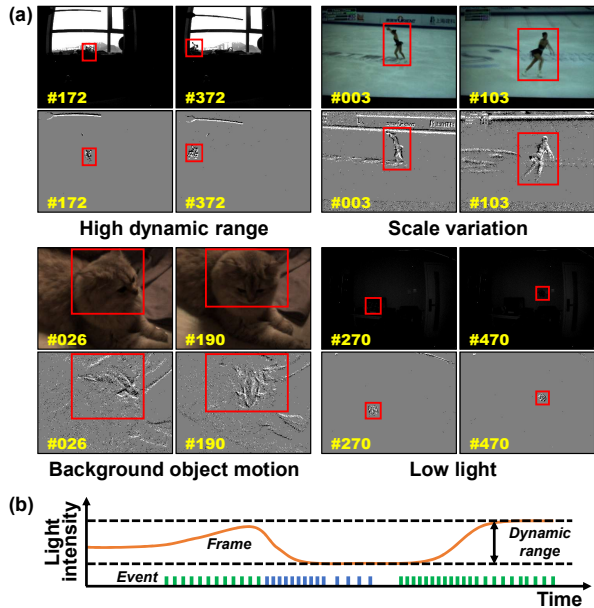


Figure 1: (a) Complementary characteristics of frame- and event-based images. Event-based cameras excel in challenging conditions, such as environments with high dynamic ranges and low light, while frame-based cameras enable the capture of rich detailed information. (b) Schematic of the imaging principle. Frame-based cameras synchronously record light intensity, while event-based cameras utilize ON/OFF spike trains to asynchronously reflect light intensity changes. Additionally, event-based cameras are compatible with higher dynamic ranges than those of frame-based cameras.

mantic segmentation [47, 3, 56, 21, 17]. In particular, large-scale frame-event-based datasets constructed using event cameras offer opportunities to perform fusion studies in related fields [44]. In this study, we leverage the strengths of both the event and frame modalities to achieve reliable object tracking.

To fully leverage the potential of multimodal data, two key challenges should be effectively addressed. (1) It is crucial to devise a hybrid feature extraction network that enables the targeted exploration of the visual cues within frame-event-based inputs. (2) To facilitate discriminative feature modeling, a novel framework for performing feature alignment and fusion is essential. We note that several studies have begun to explore the relevant problems. To process data with diverse modalities, researchers have proposed specific task-oriented networks for feature extraction purposes [53, 54]. However, these networks generally possess complex architectures and information interactions. Furthermore, a simple yet efficient approach for decoupling the spatiotemporal features contained in event data is still lacking, which also imposes a bottleneck on the subsequent feature fusion process. Researchers must integrate all

visual cues through local communication conducted on separate information channels rather than in a unified feature space. This may result in fusion modules that lack global awareness and are unable to fairly assess the relationships between different features.

To address the above challenges, we propose a novel multimodal hybrid tracker (MMHT) to effectively integrate information from two visual modalities for reliable object tracking. We develop two key components in the MMHT: multimodal feature extraction (MMFE) and transformer-based feature fusion (TFF) modules. (1) MMFE: Conventional artificial neural networks (ANNs) have demonstrated robust and excellent capabilities in terms of processing the visible light modality [31, 48, 32]. Brain-inspired spiking neural networks (SNNs) have the ability to synchronously perceive spatiotemporal features, making them suitable for neuromorphic event data [49, 29]. Therefore, we propose a hybrid network that combines ANNs and SNNs to extract multimodal features, thereby constructing a multiscale and multidimensional visual representation space. By introducing a newly developed synapse-threshold synergistic learning approach for SNNs [33], the MMFE module can optimize the network parameters in an end-to-end manner and achieve excellent performance. (2) TFF: Recently, the transformer architecture, which utilizes self-attention for global information modeling, has demonstrated remarkable capabilities in various intelligent tasks and has gained increasing attention [35, 9, 2]. Importantly, transformers are applicable to different modalities, providing a concise and efficient unified framework for multimodal fusion. Here, we construct the TFF module based on enhanced transformers by introducing a cross-attention mechanism. With the TFF module, we can align the visual representations derived from different modalities and achieve feature modeling across different domains. Accordingly, the superiority of the MMFE and TFF modules establishes a foundation for achieving reliable object tracking.

Our contributions in this paper are presented as follows:

- We propose a novel MMHT model for reliably performing single object tracking by jointly exploiting the frame and event domains.
- We design a hybrid ANN-SNN frame-event-based feature extraction approach to construct a multiscale and multidimensional visual representation space.
- We develop an enhanced transformer-based feature

fusion strategy that operates across domains to perform discriminative feature modeling.

- Experiments show that the MMHT model achieves competitive performance in comparison with that of other state-of-the-art models on challenging benchmark datasets (FE108, COESOT and VisEvent).

2. Related Works

In this section, we briefly review the recent works conducted on multimodal object tracking, multimodal feature modeling and frame-event-based object tracking, which are highly associated with our study.

2.1. Multimodal Object Tracking

To cope with complex scenarios, an increasing number of modalities are being incorporated into object tracking tasks to enable robust and comprehensive feature modeling. Currently, the most valuable modalities for research include the thermal, depth, event, and language modalities [49, 57, 23]. The thermal modality detects the surface temperature distribution of an object through thermal radiation, and its imaging process remains unaffected by weather conditions. Therefore, the thermal modality is often employed to complete tracking tasks in extreme weather conditions. However, the thermal modality also has drawbacks in terms of resolution and noise, thereby making RGB-T fusion a popular research topic in the object tracking field [41]. The depth modality constructs a 3D spatial relationship by recording the distances from objects to the camera, exhibiting excellent representation capabilities for cases with object occlusion. RGB-D fusion has demonstrated a significant impact in fields such as autonomous driving and facial detection [42]. In contrast, an event camera captures light intensity changes at a high frequency and exhibits high sensitivity to object motion. By incorporating the event modality, trackers can obtain stable object-oriented spatiotemporal features [5]. Therefore, researchers have begun exploring frame-event-based tracking, and several large-scale datasets have been released to validate the performance of the developed trackers [36, 34, 53].

2.2. Multimodal Feature Modeling

To achieve reliable feature modeling through complementary advantages, a multimodal model typically consists of three components: feature extraction, feature

alignment, and feature fusion modules. The most common feature extraction strategy involves using specialized dual-stream architectures inspired by prior knowledge based on different modalities [49, 53, 18]. This approach circumvents the challenge of designing models for inconsistent data formats while ensuring the completeness and relevance of the feature extraction process. Although some approaches consciously align their features during the extraction stage, most models still require a feature space transformation as a foundation for performing feature fusion. Generally, adaptive feature modulation and high-dimensional kernel projection are common techniques employed for feature alignment [52, 49]. In terms of feature fusion, a variety of techniques, ranging from simple feature combinations or concatenations to attention-based enhancements, have proven to be effective at leveraging the advantages of multimodal data [36]. Furthermore, inspired by transformer-based architectures, some researchers have begun exploring the possibility of constructing a unified framework [57, 34]. Their aim is to utilize an improved transformer, that encompasses all the aforementioned steps to directly accomplish feature modeling.

2.3. Frame-Event-Based Object Tracking

Tracking methods based on frame-event-based modalities have demonstrated remarkable capabilities in terms of leveraging extreme lighting conditions and extracting detailed texture information [52, 45, 53, 57, 10]. However, due to the structural differences between the information representations of these two modalities, it is crucial to design architectures that can effectively explore potential complementary task-oriented features.

Inspired by the hypothetical two-stream model of visual neural processing [11], prior studies have proposed various two-branch architectures for performing targeted feature extraction in different modalities. To achieve effective environmental perception in extreme scenarios, some existing approaches consider the event-based modality as a complement to the conventional frame-based modality. These methods focus on implementing cross-modal enhancements at the feature level [52, 36, 37] or employ hybrid architectures that combine SNNs, ANNs and hard attention mechanisms to facilitate efficient feature interaction [45, 55, 37]. Other works have aimed to provide more reliable feature cues for object tracking by delving into the temporal properties of the event modality using recurrent neural network (RNN)-like structures [53]. This strategy extends the scope of feature mining from the original spatial dimension to the spatiotemporal dimension.

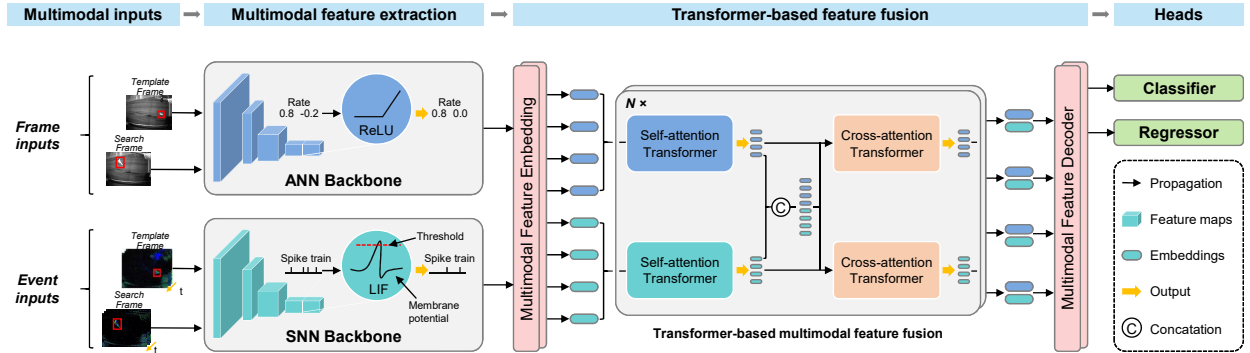


Figure 2: The overall framework of the proposed MMHT. Frame- and event-modality inputs are initially processed by hybrid backbones to extract discriminative features. These features are subsequently embedded as patch embeddings using the multimodal feature embedding module, enabling effective cross-modal visual cue alignment. The proposed transformer-based multimodal feature fusion blocks leverage diverse attention modules to enhance and seamlessly integrate cross-domain features. Ultimately, the multimodal feature decoder produces fusion-level inputs, which are employed by our heads to perform accurate object tracking.

As with other studies concerning multimodal object tracking, some researchers have highlighted the simultaneous extraction of frame-event-based features using a unified framework structured with transformers [34, 57, 50]. Remarkably, these models have exhibited competitive performance on several mainstream large-scale datasets in comparison with that of two-branch models. For instance, a novel plug-and-play mask modeling strategy has been developed in a recent study [58]. By combining with a pretrained vision transformer, this strategy can lead to notable performance enhancements for unified frameworks in object tracking tasks.

3. Methods

3.1. Overview

We first provide an overview of the proposed MMHT model. Briefly, the MMHT model evolves on the basis of discriminative correlation filter trackers, which are characterized by a shared target-specific feature extraction network and available online learning heads [6, 1]. To achieve superior multimodal feature modeling capabilities, we propose a pioneering hybrid architecture that can effectively capture cross-domain visual cues. As depicted in Fig. 2, the framework of the MMHT model includes four parts: multimodal inputs, a multimodal feature extraction module, a transformer-based feature fusion module, and heads. Notably, the MMHT model is trainable in an end-to-end trainable manner.

3.2. Multimodal Inputs

The bioinspired neuromorphic camera facilitates the simultaneous acquisition of frame-event-based data.

The conventional frame-based input $f_i(x, y)$ captures the light intensity at the i -th exposure time T_i , where (x, y) denotes the pixel location. In contrast, the event-based inputs $\{(x_k, y_k, t_k, p_k)\}_{k=1}^K$ asynchronously record light intensity changes with their polarity ($p_k \in \{-1, +1\}$). K denotes the number of events, and t_k is the corresponding timestamp of the k -th event. For convenience, the event inputs are aggregated into a frame-based representation $g_{i,j}(x, y)$ as depicted in the following formulas:

$$g_{i,j}(x, y) = [p_k \times \delta(t_{\max} - t_k) + 1] \times 127, \quad (1)$$

with

$$t_{\max} = \max \{-1, t_k \times \delta(x - x_k, y - y_k)\}, \quad (2)$$

subjected to $\forall t_k \in [T_i + jB, T_i + (j+1)B]$. In Eqs. (1) and (2), $g_{i,j}(x, y)$ represents the j -th aggregated frame during time period $[T_i, T_{i+1}]$ [53], $B = (T_{i+1} - T_i)/N$ denotes a time window with a temporal resolution of N , and δ is the Dirac delta function. In our present study, multimodal inputs are represented as a series of combinations $[(f_i, g_{i,1}, \dots, g_{i,N})]_{i=0}^I$.

3.3. Multimodal Feature Extraction

It is widely acknowledged that frame-based images possess the ability to objectively capture abundant texture information, thereby offering valuable visual cues for spatial feature modeling [8]. Nevertheless, event-based data capture object-oriented edge and motion information across the spatiotemporal domain [44], and both types of information are of equal importance for object tracking tasks. To efficiently extract diverse visual cues from multimodal inputs, we propose a novel hybrid backbone constructed with convolutional neural networks based on distinct types of neurons.

Algorithm 1 Multimodal Feature Embedding

Inputs: Feature maps $X^{C \times H \times W}$ **Parameters:** Feature patch's resolution p and embedding dimensionality D_{dim} **Output:** The embedding

- 1: Reshape $X^{C \times H \times W}$ to $X^{N \times (p^2 \cdot C)}$ # $N = H \cdot W / p^2$
 - 2: $X^{N \times (p^2 \cdot C)} \leftarrow \text{LayerNorm}(p^2 \cdot C) : X^{N \times (p^2 \cdot C)}$
 - 3: $X^{N \times D_{\text{dim}}} \leftarrow \text{Linear}(p^2 \cdot C, D_{\text{dim}}) : X^{N \times (p^2 \cdot C)}$
 - 4: $X^{N \times D_{\text{dim}}} \leftarrow \text{LayerNorm}(D_{\text{dim}}) : X^{N \times D_{\text{dim}}}$
 - 5: $X^{N \times D_{\text{dim}}} \leftarrow \text{Dropout} : X^{N \times D_{\text{dim}}}$
 - 6: **return** $X_{\text{embed}}^{N \times D_{\text{dim}}}$
-

Algorithm 2 Transformer-Based Multimodal Feature Fusion

Inputs: Embeddings F_{embed} and G_{embed} **Parameters:** Self-attention transformer blocks sat_1 , sat_2 , cross-attention transformer blocks cat_1 , cat_2 , and the number I of TMFF modules**Outputs:** Fusion embedding
 T_{embed}

- 1: **For** $i = 1$ to I do:
 - 2: $F_{\text{embed}} \leftarrow \text{sat}_1(F_{\text{embed}})$
 - 3: $G_{\text{embed}} \leftarrow \text{sat}_2(G_{\text{embed}})$
 - 4: $D_{\text{embed}} = \text{concat}(F_{\text{embed}}, G_{\text{embed}})$
 - 5: $F_{\text{embed}} \leftarrow \text{cat}_1(F_{\text{embed}}, D_{\text{embed}})$
 - 6: $G_{\text{embed}} \leftarrow \text{cat}_2(G_{\text{embed}}, D_{\text{embed}})$
 - 7: **end for**
 - 8: $T_{\text{embed}} = \text{concat}(F_{\text{embed}}, G_{\text{embed}})$
 - 9: **return** T_{embed}
-

3.3.1. ANN Backbones for the Frame Modality

The pretrained ResNet18 (structured with conv1, conv2_x, conv3_x, conv4_x, conv5_x and fully connected layers) model demonstrates powerful transferability in downstream visual tasks [12]. Thus, we adopt the convolutional layers of ResNet18 as backbones for the frame modality. The feature maps generated by conv3_x and conv4_x are used as the low-level and high-level features (F_l^i, F_h^i), respectively.

$$F_l^i = \text{conv3_x}(\text{conv2_x}(\text{conv1}(f_i))), \quad (3)$$

$$F_h^i = \text{conv4_x}(F_l^i). \quad (4)$$

3.3.2. SNN Backbones for the Event Modality

SNNs form a new generation of neural network models that leverage bioinspired neurons and discrete spike trains to mimic the intricate spatiotemporal dynamic processes observed in the human brain [27]. SNNs

Algorithm 3 Multimodal Feature Decoder

Inputs: Embeddings $X^{2N \times D_{\text{dim}}}$ **Parameters:** Feature map resolution W and H **Output:** Feature maps

- 1: $X^{2N \times D_{\text{dim}}} \leftarrow \text{LayerNorm}(D_{\text{dim}}) : X^{2N \times D_{\text{dim}}}$
 - 2: Reshape $X^{2N \times D_{\text{dim}}}$ to $X^{D_{\text{dim}} \times 2N}$
 - 3: $X^{D_{\text{dim}} \times H \cdot W} \leftarrow \text{Linear}(2N, HW) : X^{D_{\text{dim}} \times 2N}$
 - 4: $X^{D_{\text{dim}} \times H \cdot W} \leftarrow \text{LayerNorm}(HW) : X^{D_{\text{dim}} \times H \cdot W}$
 - 5: $X^{D_{\text{dim}} \times H \cdot W} \leftarrow \text{Dropout} : X^{D_{\text{dim}} \times H \cdot W}$
 - 6: Reshape $X^{D_{\text{dim}} \times H \cdot W}$ to $X^{D_{\text{dim}} \times H \times W}$
 - 7: **return** $X^{D_{\text{dim}} \times H \times W}$
-

have garnered significant attention due to their exceptional proficiency in extracting spatiotemporal features [47, 51, 26]. In this study, we employ the leaky integrate and fire (LIF) neuron, a computational model that strikes a balance between dynamic complexity and computational simplicity, to construct SNN backbones for extracting features from the event modality. Without loss of generality, the iterative form of the LIF neuron utilized in our work can be described as follows:

$$u^t = \alpha \cdot (1 - o^{t-1}) \cdot u^{t-1} + \sum_{m=1}^M w_m \cdot o_m^t, \quad (5)$$

$$o^t = \sigma(u^t - u_{\text{th}}), \quad (6)$$

where u^t and o^t represent the neuronal membrane potential and spike output at time t , respectively. In addition, α and u_{th} are intrinsic neuronal properties: the membrane decay constant and spike threshold, respectively. w_m denotes the synaptic weight. In this study, we use a novel proposed synapse-threshold synergistic learning approach to simultaneously train w_m and u_{th} for SNNs [33].

The architectures of the backbones comprise convolutional layers (convl_x, convh_x) structured in the form of the feature extraction component in AlexNet [20]. These architectures undergo meticulous refinement and optimization to suit a variety of datasets and accommodate feature fusion modules (detailed parameters are listed in Tab.1). To obtain low-level and high-level spiking feature trains ($[G_{l,1}^i, \dots, G_{l,N}^i]$, $[G_{h,1}^i, \dots, G_{h,N}^i]$), the following procedure is employed:

$$[G_{l,1}^i, \dots, G_{l,N}^i] = \text{convl_x}([g_{l,1}, \dots, g_{l,N}]), \quad (7)$$

$$[G_{h,1}^i, \dots, G_{h,N}^i] = \text{convh_x}([G_{l,1}^i, \dots, G_{l,N}^i]). \quad (8)$$

Utilizing the average firing rate observed over $[T_i, T_{i+1}]$, we code and normalize the spiking feature maps as feature maps G_l^i and G_h^i :

$$G_l^i = \frac{1}{N} \sum_{n=1}^N G_{l,n}^i, \quad (9)$$

$$G_h^i = \frac{1}{N} \sum_{n=1}^N G_{h,n}^i. \quad (10)$$

To address the nondifferential nature of spiking events, we employ an approximate gradient function during the feedback propagation process [38, 39]:

$$\sigma' = \text{ReLU}(1 - |x|), \quad (11)$$

where ReLU represents the activation function of the rectified linear unit.

3.4. Transformer-Based Feature Fusion

Our proposed method aims to efficiently fuse visual cues in the complete feature space through an improved transformer-based module.

3.4.1. Multimodal Feature Embedding

To obtain modality-independent formalized embeddings, we introduce a novel feature embedding process in our approach. It consists mainly of reshaping conversion operations and a linear layer, which can effectively convert the original features into constant latent vectors while mitigating any potential inductive bias [35]. The specific process and parameters are outlined in Algorithm 1 and Tab.1, respectively. Therefore, the feature maps derived from different modalities (G_1^i , F_1^i , G_h^i and F_h^i) are transformed into uniform embeddings ($G_{1,\text{embed}}^i$, $F_{1,\text{embed}}^i$, $G_{h,\text{embed}}^i$ and $F_{h,\text{embed}}^i$). Note that the numbers and dimensions of the embeddings are equivalent across different modalities within our study.

3.4.2. Transformer-Based Multimodal Feature Fusion

The framework of the transformer-based multimodal feature fusion module comprises two self-attention transformer (sat) blocks, two cross-attention transformer (cat) blocks, and two concatenation operation (concat), as shown in Algorithm 2.

The sat blocks employ standard transformers, which are characterized by multihead self-attention (MSA) and multilayer perceptrons (MLP), to enhance the feature patch embeddings [9]:

$$\tilde{X} = \text{MSA}(\text{LN}(X)) + X, \quad (12)$$

$$X = \text{MLP}(\tilde{X}) + \tilde{X}. \quad (13)$$

Here, LN represents the Layer Normalization operation, and X denotes the input patch embeddings. In each cat block, a modified cross-attention (CA) mechanism is utilized to replace the self-attention in MSA:

$$\text{CA} = \text{softmax}\left(\frac{XD^T}{\sqrt{D_{\text{dim}}}}\right) \times D, \quad (14)$$

where $X^{N \times D_{\text{dim}}}$ denotes the enhanced embeddings and $D^{2N \times D_{\text{dim}}}$ represents the fusion embeddings. In a certain sense, the proposed CA mechanism facilitates the extensive target-specific modeling of visual cues across different domains. Using the MLP and multihead cross-attention (MCA) refined with ca mechanism, the entire process of cat block can be described as follows:

$$\tilde{X} = \text{MCA}(\text{LN}(X)) + X, \quad (15)$$

$$X = \text{MLP}(\tilde{X}) + \tilde{X}. \quad (16)$$

Similar to a general transformer encoder, our feature fusion module also enables repetitive embedding processes.

To date, the fusion patch embeddings of low-level $T_{1,\text{embed}}^i$ and high-level $T_{h,\text{embed}}^i$ are obtained:

$$T_{1,\text{embed}}^i = \text{Algorithm2}(F_{1,\text{embed}}^i, G_{1,\text{embed}}^i), \quad (17)$$

$$T_{h,\text{embed}}^i = \text{Algorithm2}(F_{h,\text{embed}}^i, G_{h,\text{embed}}^i). \quad (18)$$

3.4.3. Multimodal Feature Decoder

To provide inputs for the tracking heads, we design a multimodal feature decoder to convert the embeddings into fusion-level feature maps (given in Algorithm 3). In our decoder, the embeddings in each dimension are projected into a new feature space using a linear layer, and its distribution is adjusted by layer normalization. To date, multimodal feature modeling has been accomplished, yielding fusion-level feature maps T_1^i and T_h^i .

3.5. Heads and Loss

For the tracking heads, namely, the regressor and classifier, we employ the target estimation network from ATOM [6] and the classifier from DiMP [1], respectively. The regressor, characterized by modulation (IoU_{mod}) and prediction (IoU_{pre}) blocks, takes as low-level and high-level feature maps (T_1^i and T_h^i , respectively) as inputs to estimate IoU^i . Mathematically, the computational procedure can be expressed as follows:

$$v_1, v_h = IoU_{\text{mod}}(T_{1,t}^i, T_{h,t}^i, B_t), \quad (19)$$

$$IoU^i = IoU_{\text{pre}}(T_{1,s}^i, T_{h,s}^i, B_s, v_1, v_h). \quad (20)$$

Here, subscript t and s denote template and search frame, respectively. The symbol B represents the target bounding box. On the other hand, the classifier utilizes T_h^i to predict a confidence score s^i for the target as follows:

$$s^i = \text{Classifier}(T_{h,t}^i, T_{h,s}^i, B_t). \quad (21)$$

Table 1: Details of model configurations for different datasets. In the MMFE module, for example, C64k11s4p5 signifies a convolutional layer with 64 output channels, kernel size 11, stride 4, and padding 5. BN represents batch normalization. In the TFF module, parameters include the resolution of feature patches p , the embeddings dimensionality D_{dim} and the number of heads in MSA and MCA.

Datasets	MMFE		TFF (#Block = 2)		
	ConvL_x	ConvH_x	p	D_{dim}	#head
FE108	C64k11s4p5-BN-C128k5s2p2-BN-C128k3s1p1-BN	C256k3s2p1-BN	4	512	2
VisEvent	C64k11s4p5-C128k5s2p2	C256k3s2p1	4	512	2
COESOT	C64k11s4p5-C128k5s2p2	C256k3s2p1	4	512	2

Table 2: Comparison among the existing large-scale frame-event-based datasets for object tracking. The # symbol represents the number of corresponding items.

Datasets	Year	#Videos	#Train/Test	#Frames	Resolution	#Attributes	Device
FE108	2021	108	76/32	200157	346×260	4	DAVIS346
VisEvent	2021	746	445/301	323220	346×260	17	DAVIS346
COESOT	2022	1354	827/527	466833	346×260	17	DAVIS346

Notably, the discriminative filter generated in the classifier can be learned online.

The loss function L_{total} for offline training is defined as follows:

$$L_{total} = \beta L_{cls} + L_{reg}, \quad (22)$$

with

$$L_{cls} = \frac{1}{I} \sum_{i=1}^I \zeta^2(s^i, s_{gt}^i), \quad (23)$$

$$\zeta(s^i, s_{gt}^i) = \begin{cases} s^i - s_{gt}^i, & \text{if } s_{gt}^i > 0.05 \\ \max(0, s^i), & \text{if } s_{gt}^i \leq 0.05 \end{cases}, \quad (24)$$

$$L_{reg} = \frac{1}{I} \sum_{i=1}^I (IoU^i - IoU_{gt}^i)^2, \quad (25)$$

where s_{gt}^i is a Gaussian label generated according to the corresponding ground truth IoU_{gt}^i . The losses of the classifier L_{cls} and regressor L_{reg} represent the mean squared error determined on I samples. The constant coefficient β is used to balance the weight between two heads.

4. Experiments

In this section, we begin by providing a comprehensive overview of our experimental settings, encompassing the utilized datasets, evaluation metrics, and preprocessing steps. Subsequently, we present a detailed performance comparison between our proposed MMHT model and other state-of-the-art models on diverse benchmark datasets. Furthermore, we conduct rigorous ablation studies to demonstrate the indispensability of multimodal tracking, the hybrid backbones, and the proposed fusion components. To achieve enhanced comprehension, representative figures are given to provide qualitative visualizations.

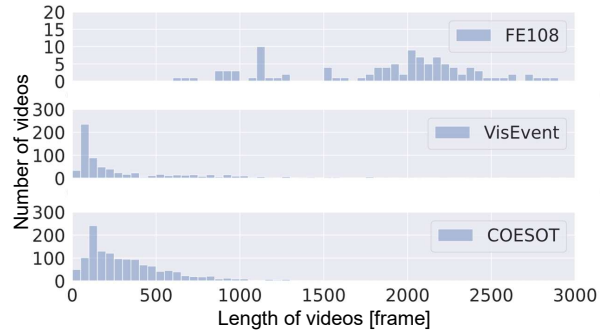


Figure 3: The video length distribution across the datasets, with a histogram interval of 50 frames and an upper bound of 3000 frames in the statistics.

4.1. Experimental Settings

4.1.1. Datasets

In our experiments, the FE108 [53], VisEvent [36] and COESOT [34] datasets, captured in real scenes using a DAVIS346 event camera, are utilized to train and test our trackers. The DAVIS346 camera enables the simultaneous acquisition of aligned frame-event-based data with a spatial resolution of 346×260.

As the details of the datasets shown in Tab. 2, the FE108 dataset consists of 108 annotated videos, with 72 videos used for training and 32 videos employed for testing. These videos are categorized based on four attributes: low light (LL), high dynamic range (HDR), fast motion with motion blur (FWB), and fast motion without motion blur (FNB). The VisEvent dataset, which is also used in our work, includes 746 annotated videos, with 445 videos for training and 301 videos for testing. The COESOT dataset comprises 1354 annotated videos, with 827 videos for training and 527 videos for testing. Notably, due to missing raw data

Table 3: Comparison among the state-of-the-art performance metrics, including PR, SR, OP50, OP75 and FPS, achieved on the FE108, COESOT and VisEvent. The average results obtained by the MMHT model are presented as means \pm standard deviations. The best results are emphasized in bold. The annotations of the CEUT model indicate different data processing approaches. Note: The ATOM and PrDiMP models were originally proposed in Ref. [6] and Ref. [7], respectively.

Method	Fusion level	PR[%]	SR[%]	OP50[%]	OP75[%]	FPS
FE108						
ATOM+Event [53]	data-level	81.80	55.50	70.00	27.40	-
PrDiMP+Event [53]	data-level	87.70	59.00	74.40	29.80	-
CEUT ₁ [34]	unified backbone	84.46	55.58	-	-	-
RT-MDNet [36]	feature-level	56.40	35.90	-	-	14
CDFI [53]	feature-level	92.40	63.40	81.30	34.40	30
MMHT (Ours)	feature-level	93.62\pm.33	62.97 \pm .11	81.68\pm.26	29.92 \pm .15	17
COESOT						
OTrack [48]	data-level	66.60	59.00	-	-	105
SiamR-CNN+Event [34]	data-level	67.50	60.90	-	-	5
KeepTrack+Event [34]	data-level	66.10	59.60	-	-	18
CEUT ₁ [34]	unified backbone	70.50	62.00	-	-	75
CEUT ₂ [34]	unified backbone	68.60	60.40	-	-	-
MDNet-MF [34]	feature-level	64.70	56.30	-	-	14
MMHT (Ours)	feature-level	74.03\pm.20	65.81\pm.12	77.64\pm.12	56.97\pm.14	19
VisEvent						
CEUT ₁ [34]	unified backbone	69.06	53.12	-	-	-
ViPT [57]	unified backbone	75.80	59.20	-	-	-
Un-Track [40]	unified backbone	76.30	59.70	-	-	-
ProTrack [43]	prompt-based	61.70	47.40	-	-	-
SiamFC [15]	feature-level	52.30	35.00	-	-	-
AFNet [52]	feature-level	59.30	44.50	-	-	-
MMHT (Ours)	feature-level	73.26 \pm .11	55.10 \pm .16	65.94 \pm .20	42.78 \pm .14	21

and annotations, we refilter the VisEvent dataset. Both datasets cover 17 representative attributes. However, our work focuses on four specific attributes: background object motion (BOM), background clutter (BC), scale variation (SV), and viewpoint change (VC).

Additionally, we analyze the video lengths distributions of the three datasets. As depicted in Fig. 3, the FE108 dataset has the fewest number of videos but the longest video length. On the other hand, the VisEvent and COESOT datasets exhibit centralized video length distributions, with videos mostly within 500 frames. These datasets provide a comprehensive understanding of the performance achieved by the model in both long- and short-term tracking scenarios.

4.1.2. Evaluation Metrics

To validate the performance of our trackers, we plot the precision and success curves of our testing results. The precision curve illustrates the percentage of frames where the center distance between the predicted and ground-truth bounding boxes falls within a specified threshold. The success curve focuses on the frames where the overlap between the predicted and ground-truth bounding boxes exceeds a given threshold. In our study, we employ several quantitative metrics for evaluation purposes: the precision rate (PR) measured with 20 pixels as the threshold; the success rate (SR) rep-

resented by the area under the success curve; and two overlap precision rates (OP50 and OP75), indicating the success rates achieved at overlap levels of 0.50 and 0.75, respectively.

4.1.3. Implementation Details

The MMHT model is implemented using PyTorch and executed on a workstation equipped with NVIDIA A100 GPUs. The training process of our trackers consists of 50 epochs, with a batch size of 20 and the adaptive moment estimation (Adam) optimizer [19] with its default parameters. For the FE108 dataset, the initial learning rates of the hybrid backbones and the other components are set to 0.0001 and 0.001, respectively. For the VisEvent and COESOT datasets, the ANN backbone has an initial learning rate of 0.00001, but the other parameters are set to 0.001. In the SNN backbones, all trainable spike thresholds u_{th} are initialized to 1.0, and the membrane decay constant α is fixed at 0.7. All the learning rates follow the exponential decay process with a factor of 0.9. All trackers are tested 5 times, and the reported results are averaged. The code of our implementation will be available at <https://github.com/GuoLab-UESTC> after this manuscript is accepted for publication.

Table 4: Analysis of the performance achieved by trackers trained with single-modal and multimodal data. The left section showcases the comprehensive evaluation results, while the right section provides specific comparisons pertaining to typical diverse attributes.

FE108	Modality	Attributes									
		ALL		LL		HDR		FWB		FNB	
		PR[%]	SR[%]	PR[%]	SR[%]	PR[%]	SR[%]	PR[%]	SR[%]	PR[%]	SR[%]
Frame	72.48±.44	48.48±.25	43.59±1.07	29.09±.64	62.11±.83	40.56±.46	99.72±.04	68.22±.05	94.78±.35	62.22±.22	
Event	84.18±.50	55.44±.30	96.19±.20	66.00±.21	81.84±.27	52.06±.17	100.00±.00	69.83±.05	62.51±2.10	35.64±1.07	
Fusion	93.62±.33	62.97±.11	96.37±1.20	66.02±.73	89.43±.54	58.13±.23	99.80±.02	71.34±.06	95.53±.36	61.93±.18	
COESOT	Modality	Attributes									
		ALL		BOM		BC		SV		VC	
		PR[%]	SR[%]	PR[%]	SR[%]	PR[%]	SR[%]	PR[%]	SR[%]	PR[%]	SR[%]
Frame	66.16±.20	62.51±.08	62.84±.21	60.65±.08	50.82±.36	48.51±.18	68.08±.50	64.92±.38	62.97±.68	60.89±.64	
Event	52.34±.16	52.98±.12	50.03±.27	52.31±.20	43.66±.26	43.84±.23	47.87±.35	50.07±.14	45.50±.65	50.25±.53	
Fusion	74.03±.20	65.81±.12	73.20±.25	65.52±.13	67.41±.41	57.53±.21	71.51±.29	65.38±.18	67.20±.24	64.61±.15	
VisEvent	Modality	Attributes									
		ALL		BOM		BC		SV		VC	
		PR[%]	SR[%]	PR[%]	SR[%]	PR[%]	SR[%]	PR[%]	SR[%]	PR[%]	SR[%]
Frame	69.26±.10	52.84±.15	65.27±.20	49.73±.14	65.23±.20	49.10±.22	62.30±.14	48.07±.19	58.66±.09	46.56±.26	
Event	62.70±.14	48.47±.22	57.69±.23	44.74±.04	57.36±.19	44.42±.22	58.73±.14	45.72±.16	53.59±.26	42.72±.17	
Fusion	73.26±.25	55.10±.15	69.75±.16	52.42±.08	70.10±.23	51.83±.08	67.33±.15	50.58±.22	68.40±.11	52.44±.11	

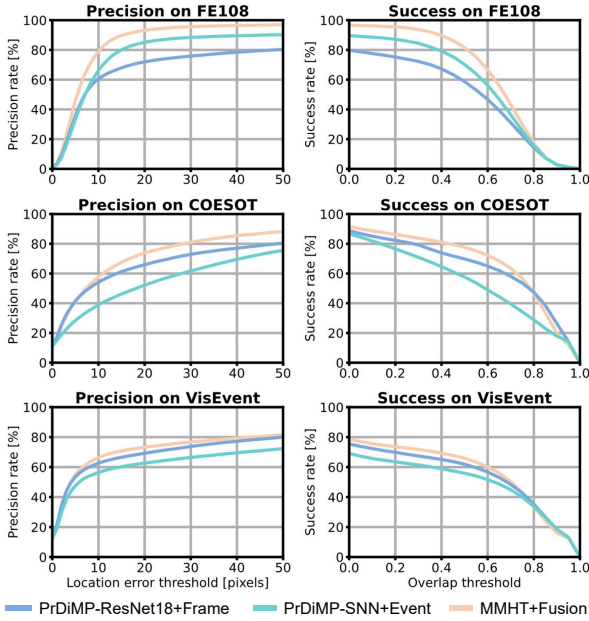


Figure 4: The precision and success curves yielded by trackers trained with different modalities.

4.2. Comparison with the State-of-the-Art Methods

To validate the effectiveness of our proposed MMHT, we conduct a comparative analysis with other state-of-the-art trackers [53, 34, 36, 48, 52, 43, 15] on the FE108, COESOT, and VisEvent datasets. According to their fusion levels, these trackers can be classified into various categories: data-level fusion trackers (where data from multiple sources are combined at the input layer), feature-level fusion trackers (where features are separately extracted from different modalities and combined

to create a unified representation for tracking purposes), unified backbone fusion trackers (which utilize a single backbone network to process data from multiple modalities), and prompt-based fusion trackers (where multiple modalities serve as a prompt guide for reliable visible image tracking).

As shown in Tab. 3, the MMHT outperforms the other methods on both the FE108 and COESOT datasets in terms of a majority of the utilized metrics. Notably, on the FE108 dataset, the MMHT achieves a 1.22% PR improvement and a 0.38% OP50 improvement over the previous best method. On the COESOT dataset, our model demonstrates PR and SR improvements of 3.53% and 3.81%, respectively. To our knowledge, our work is the first to publish OP50 and OP75 results obtained on the COESOT dataset. On the VisEvent dataset, our MMHT model yields slightly lower PR and SR results than those of the current state-of-the-art method (i.e., see ViPT and Un-Track in Tab. 3). To a certain extent, this might be due to the partial absence of raw data in the VisEvent dataset, causing different models to use different numbers of training and test samples in the experiments. Furthermore, by comparing the distributions of video lengths reported in the previous study [36], the absent data primarily concentrates in long videos exceeding 1000 frames. Considering the substantial improvement of MMHT on datasets FE108 and COESOT with a higher proportion of long videos, we posit that the absence of long videos may also impact the evaluation performance of MMHT. Remarkably, when compared to the existing state-of-the-art feature-level fusion trackers, we find that the MMHT achieves notable PR advancements (with a substantial increase of 13.96%) and

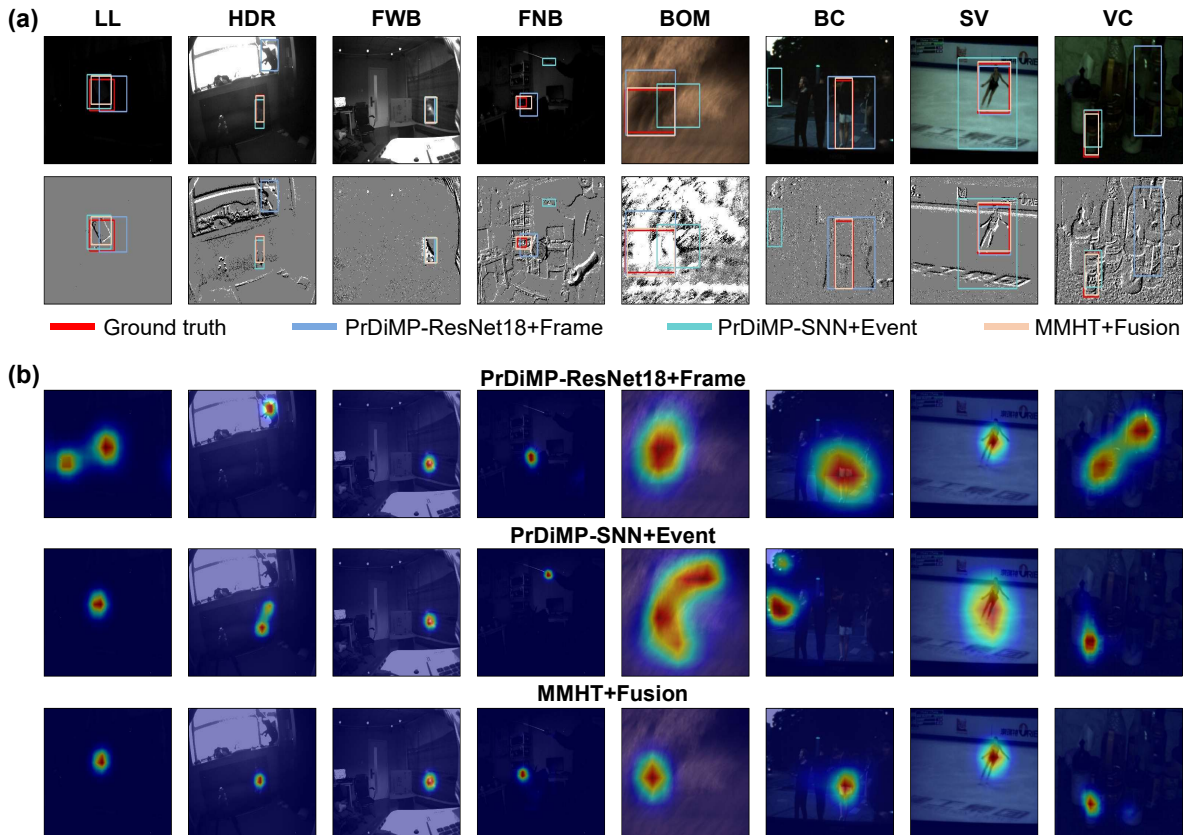


Figure 5: Visualization of the results produced by trackers trained using diverse modalities. (a) Tracking results obtained from trackers trained with various modalities. The predicted bounding boxes generated by the trackers are visually compared with the ground truth bounding boxes of the input images obtained from two modalities. (b) Corresponding response maps of different trackers. The response intensity progresses from green to red, indicating an increasing response level.

a significant SR improvement (with a boost of 10.60%).

Tracking speed, commonly quantified in frames per second (FPS), is a crucial metric for evaluating tracker performance in real applications. As illustrated in Tab. 3, the tracking speeds of the MMHT model (17, 19, and 21 FPS on FE108, COESOT, and VisEvent, respectively) fall within the mid-range and are just lower than those of specific models (CDFI 30 FPS, OSTRack 105 FPS, and CEUT 75 FPS). It is evident that such intermediate performance of the MMHT model in tracking speed is attributable to the increased computational complexity introduced by the two-stream hybrid strategy. However, by considering the significant accuracy improvements of the model on different datasets, we posit that the tracking speeds of MMHT are still acceptable for real applications.

Overall, these observations demonstrate the superiority of our proposed MMHT model, which can exhibit competitive performance in comparison with that of

previously developed state-of-the-art methods on various benchmark datasets.

4.3. Ablation Studies

4.3.1. Analysis of the Visual Modality

To further illustrate the benefits of employing multimodal data for object tracking, we conduct an ablation analysis on trackers trained exclusively on single-modal data. Specifically, we retain corresponding input and backbone modules in MMHT tailored to the utilized modality. The TFF module is removed, while the tracking heads remain unaltered. In these single-modal trackers, denoted as PrDiMP-SNN+Event and PrDiMP-ResNet18+Frame, tracking heads directly receive both low-level and high-level features to generate predictions. The precision and success curves are depicted in Fig. 4. In summary, our multimodal MMHT models demonstrate significantly wider performance margins than those of their single-modal counterparts across

different datasets.

Quantitative comparison: The precise results are presented in Tab. 4. When employing single-modal tracking on FE108, the event modality demonstrates significant advantages over the frame modality. However, the incorporation of multimodal data still yields improvements of 9.44% and 7.53% in terms of the PR and SR metrics, respectively. On the more challenging COESOT and VisEvent datasets, the frame modality exhibits a notable advantage. Nevertheless, with the utilization of multimodal data, we observe a substantial PR and SR increase of 7.87% and 3.30% on the COESOT dataset and 4.00% and 2.26% on the VisEvent dataset, respectively. These results affirm the outstanding multimodal tracking performance of the proposed approach.

Attribute-based comparison: We roughly divide several typical attributes into two categories: 1. environment-oriented attributes, including LL, HDR, BOM, and BC, and 2. object-oriented attributes including FWB, FNB, SV, and VC. Specifically, in challenging scenarios influenced by environmental factors, the event modality exhibits pronounced advantages in scenarios with LL and HDR. This advantage stems from the higher dynamic ranges of the photodetector used by the event camera. However, in BOM and BC scenarios, the event modality may be susceptible to significant discriminative filter drift due to the absence of texture features, rendering it less effective than the frame modality. In challenging scenarios caused by the target objects, the frame modality excels in cases with FNB, SV, and VC. We posit that these scenarios may disrupt the temporal features of the event data, whereas the abundant spatial information in the frame modality remains relatively unaffected. However, in the FWB case, both single-modal trackers achieve nearly perfect scores in terms of the PR and SR metrics. Nevertheless, the multimodal MMHT still demonstrates superiority across most attributes.

Qualitative visualizations: To achieve intuitive comprehension, we randomly select a representative sample from each of the eight attributes for visual analysis purposes (4 from FE108 and 4 from COESOT and VisEvent). As illustrated in Fig. 5, we plot the tracking results (Fig. 5(a)) and corresponding response maps (Fig. 5(b)) yielded by trackers trained with diverse modalities. The visualized results align well with the quantitative findings. Except for the relatively simple FWB scenario, in which nearly no discernible differences are observed among the performances of all models, the trackers trained with a single modality exhibit instances of identification errors (HDR, FNB, BC and VC) or response drift (LL, BOM and SV) across

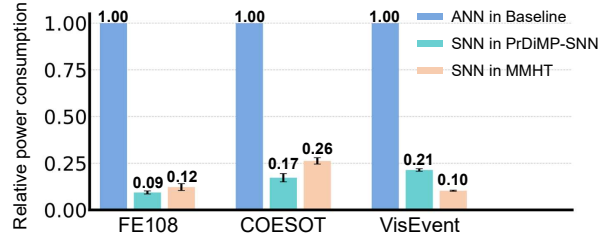


Figure 6: The relative power consumption levels of the SNN backbones for a single modality and the fusion modality.

most attributes. In contrast, the MMHT models exhibit more precise responses to objects, yielding more accurate bounding box predictions. The visualization analysis further substantiates the exceptional robustness and superiority of MMHT models in terms of achieving effective object tracking across a spectrum of challenging scenarios.

4.3.2. Analysis of the SNN Backbones for the Event Modality

To demonstrate the influence of the SNN backbone in our MMHT model, we conduct experiments focusing on both performance and power consumption.

To demonstrate the superior performance of SNN in processing event data, we replace the SNN backbone of the event modality with a structurally identical ANN in both the PrDiMP-SNN and MMHT models. Specifically, the modified models are denoted as PrDiMP-ANN (for event-modal trackers) and MMHT-ANN (for fusion trackers), respectively. A detailed performance analysis is carried out, and the overall evaluation results, measured in terms of the PR and SR metrics, are presented in Tab. 6. Notably, across various datasets, the models utilizing SNN backbones demonstrate significantly superior performance to that of the models employing ANN backbones. Specifically, on the FE108 dataset, the SNN backbones contribute to 4.21% and 4.81% PR and SR improvement for the single-modal-based tracker, and 25.37% and 18.98% improvements for the multimodal-based tracker. On the COESOT dataset, the PR and SR improvement are 1.97%, 0.2%, 3.08%, and 3.26%, respectively. On the VisEvent dataset, the PR and SR improvements are 17.22%, 12.58%, 8.02%, and 4.15%, respectively.

Furthermore, prior studies have underscored the reduced energy consumption exhibited by SNNs [46, 30, 29]. When compared with ANNs employing Multiply-Accumulate (MAC) operations as their predominant computational units, SNNs utilizing small numbers of MAC operations solely in the input layers and mainly

Table 5: The MAC and AC operations in both the ANN and SNN backbones. E_{MAC} and E_{AC} represent the empirical energy consumption values. K_n denotes the size of the convolutional kernels in the n -th layer. H , W , and C refer to the height, width, and channel dimensions of the feature maps, respectively. FR signifies the average firing rate of SNNs [4].

OPs	Power consumption	The number of OPs within backbones	
		ANN	SNN
MAC	$E_{MAC} = 4.6pJ$	$MAC_{ANN} = \sum_{n=1}^N K_n^2 \cdot C_{n-1} \cdot H_n \cdot W_n \cdot C_n$	$MAC_{SNN} = N \cdot K_1^2 \cdot C_0 \cdot H_1 \cdot W_1 \cdot C_1$
AC	$E_{AC} = 0.9pJ$	$AC_{ANN} = 0$	$AC_{SNN} = N \cdot \sum_{n=2}^N FR_n \cdot K_n^2 \cdot C_{n-1} \cdot H_n \cdot W_n \cdot C_n$

Table 6: Performance analysis of various backbones with respect to event feature extraction.

Modality	Model	PR[%]	SR[%]
FE108	Event	79.91±.34	50.63±.19
		PrDiMP-ANN	84.18±.50
		PrDiMP-SNN	55.44±.30
Fusion	MMHT-ANN	68.25±.29	43.99±.21
		MMHT	93.62±.33
		62.97±.11	
COESOT	Event	50.37±.08	52.78±.11
		PrDiMP-ANN	52.34±.16
		PrDiMP-SNN	52.98±.12
Fusion	MMHT-ANN	70.95±.29	62.55±.18
		MMHT	74.03±.20
		65.81±.12	
VisEvent	Event	45.48±.51	35.89±.37
		PrDiMP-ANN	62.70±.14
		PrDiMP-SNN	48.47±.22
Fusion	MMHT-ANN	65.24±.33	50.95±.18
		MMHT	73.26±.25
		55.10±.15	

utilizing sparse Accumulate (AC) operations lead to notable power consumption reductions. A comprehensive quantitative analysis of the operations used by both the ANN and SNN backbones is presented in Tab. 5. Additionally, we provide the empirical power consumption values for both the MAC (E_{MAC}) and AC (E_{AC}) operations executed on the chip. Subsequently, we derive the theoretical energy consumption levels of ANN (Φ_{ANN}) and SNN (Φ_{SNN}) as follows:

$$\Phi_{ANN} = E_{MAC} \cdot MAC_{ANN}, \quad (26)$$

$$\Phi_{SNN} = E_{MAC} \cdot MAC_{SNN} + E_{AC} \cdot AC_{SNN}. \quad (27)$$

Consequently, the relative energy consumption of the SNN backbones in relation to that of the ANN backbones can be defined as:

$$\eta = \frac{\Phi_{SNN}}{\Phi_{ANN}}. \quad (28)$$

Obviously, a smaller value of η means a lower energy consumption.

In experiments, we randomly select five samples from various datasets to test the firing rates (FRs) and statistic the corresponding MAC and AC operations. An illustration of the power consumption of the SNN backbones relative to that of identical ANN backbones (denoted as ‘‘ANN in Baseline’’) is presented in Fig. 6. Due to the utilization of AC operations and sparse firing rates, the SNN backbones demonstrate a substantial reduction in power consumption. Specifically, on

the FE108 and VisEvent datasets, the SNN backbones exhibit up to 0.90 power savings. On the COESOT dataset, the ratios hover around 0.80. Additionally, we also conduct a comprehensive examination to assess the energy consumption of the overall backbone within MMHT tracker. In contrast to utilizing Resnet+ANN as the backbone, the Resnet+SNN backbone demonstrates a notable energy conservation of approximately 0.10 (with specific reductions of 0.12 on FE108, 0.07 on COESOT, and 0.12 on VisEvent).

4.3.3. Effectiveness of the TFF Fusion Method

To validate the effectiveness of our proposed TFF feature fusion method, we conduct experiments encompassing an evaluation of several feature fusion approaches for comparative analysis purposes. Specifically, the following techniques are considered: (1) concatenation (referred to as ‘Concat’), which involves the concatenation of the feature maps generated from the ANN and SNN backbones along the channel dimension; (2) addition (referred to as ‘Add’), which entails the fusion of feature maps through element-wise summation at the corresponding positions; (3) point-wise convolution (denoted as ‘1×1Conv’), which is employed to consolidate features from diverse backbones by means of a 1×1 convolution on individual pixels [13]; and (4) squeeze-and-excitation attention block (denoted as ‘SE’), which is introduced to adaptively recalibrate the significance of each channel across feature maps from both modalities [14]. The detailed results obtained based on diverse fusion methods are presented in Tab. 7. In the comparative assessment of the ‘Concat’, ‘Add’, ‘1×1Conv’ and ‘SE’ methods, ‘1×1Conv’ exhibits superior performance across the majority of metrics, including PR on FE108, PR and SR on COESOT, and PR on VisEvent. Conversely, ‘SE’ yields suboptimal results, except for SR on FE108. These findings align consistently with those reported in a previous study [36]. However, the TFF method consistently exhibits superior performance across all metrics. Furthermore, in comparison with the single-modal trackers presented in Tab. 4, the multimodal trackers employing relatively simple feature fusion methods (‘Concat’, ‘Add’, ‘1×1Conv’ and ‘SE’) still demonstrate enhanced track-

Table 7: Performance analysis of various fusion method.

Method	FE108		COESOT		VisEvent	
	PR[%]	SR[%]	PR[%]	SR[%]	PR[%]	SR[%]
Concat	89.14±.85	61.70±.68	71.26±.00	65.57±.04	69.05±.30	54.60±.16
Add	90.67±.06	62.66±.03	70.19±.12	65.30±.07	69.30±.24	55.09±.25
1×1Conv	91.26±.29	62.34±.12	72.08±.21	65.63±.14	70.06±.19	54.91±.06
SE	89.58±.24	61.76±.17	69.76±.19	65.04±.16	68.92±.14	54.35±.12
TFF	93.62±.33	62.97±.11	74.03±.20	65.81±.12	73.26±.25	55.10±.15

Table 8: The effectiveness of different embedding dimension.

MFE	$D_{dim} = 256$		$D_{dim} = 512$		$D_{dim} = 1024$	
	PR[%]	SR[%]	PR[%]	SR[%]	PR[%]	SR[%]
FE108	87.21±.78	57.94±.41	93.62±.33	62.97±.11	90.60±.67	60.44±.38
COESOT	61.14±.20	56.52±.09	74.03±.20	65.81±.12	70.11±.24	63.75±.42
VisEvent	66.99±.55	48.87±.28	73.26±.25	55.10±.15	72.07±.25	54.59±.11

ing performance. This outcome serves to underscore our earlier conclusion that multimodal data provide opportunities for achieving reliable object tracking.

Moreover, we conduct an in-depth analysis of two key components within the TFF module. (1) The embedding dimensionality D_{dim} in the Multimodal Feature Embedding (MFE) plays a crucial role in influencing the sparsity of the features within the transformation space. Accordingly, by varying the size of D_{dim} , we demonstrate its impact on the TFF fusion method, as presented in Tab. 8. The experimental findings reveal that deploying a smaller embedding dimensionality leads to a notable performance decline, which is particularly evident on the COESOT dataset, with a reduction of approximately 10%. On the other hand, utilizing a larger value still results in performance degradation; however, the tracker maintains a relatively commendable performance level. We speculate that both excessively small and excessively large feature sparsity values can yield unfavorable outcomes for the model. Specifically, an excessively small D_{fc} may result in information loss during the feature transformation process, while excessive feature redundancy may impose a burden on the effectiveness of model training. (2) We also discuss the number of Transformer-based Multimodal Feature Fusion (TMFF) modules to elucidate the correlation between tracker performance and the iterative fusion process. The outcomes of the experiments are presented in Tab. 9, revealing the noteworthy influences of varying numbers of fusion iterations on the ultimate performance of the model. For the FE108 and COESOT datasets, the model attains its optimal performance with 2 fusion iterations. However, in the case of the VisEvent dataset, the performance of the model demonstrates approximate equivalence between 1 and 2 fusion iterations. Combining the experimental findings

observed in this section, the MMHT model proposed in this manuscript is characterized with the following parameters $D_{dim}=512$ and #Block=2.

4.4. Multimodal Feature Fusion on the MMHT

To demonstrate the operational mechanisms of the proposed MMHT model, we visualize the feature maps extracted from the hybrid backbone and the attention maps generated by the fusion module. Specifically, to compare the functional disparities of backbones in capturing visual cues, we randomly select feature maps from the representative channels in F_h^i and G_h^i , respectively. Regarding the fusion module, we initially compute the average of the fusion embeddings $G_{h,embed}^i$ and $F_{h,embed}^i$ along the dimensional direction. Subsequently, attention maps are derived by retaining only the significant regions where the value exceeds 0.5. As shown in Fig. 7, the ANN backbone effectively captures intricate texture features from the frame modality, while the SNN backbone exhibits heightened sensitivity toward moving objects. By integrating multimodal features, the fusion module precisely focuses its attention on the target object and crucial background information, thereby enhancing the reliability of object tracking. To a certain extent, our observation demonstrates that the MMHT model can effectively fuse multimodal features across different domains.

5. Conclusion

In this paper, we proposed a novel MMHT model, aiming to exploit the potential of diverse visual modalities to achieve reliable single object tracking. Specifically, we designed a hybrid backbone that enables the extraction of features from multiple visual modalities. By aligning and mapping visual features from different

Table 9: The effectiveness of varying numbers of fusion iterations.

TMFF	#Block=1		#Block=2		#Block=3	
	PR[%]	SR[%]	PR[%]	SR[%]	PR[%]	SR[%]
FE108	81.20±1.07	52.42±.60	93.62±.33	62.97±.11	82.53±.40	53.92±.14
COESOT	68.60±.13	62.60±.08	74.03±.20	65.81±.12	68.67±.32	61.02±.26
VisEvent	71.81±.25	55.86±.09	73.26±.25	55.10±.15	62.56±.27	44.31±.12

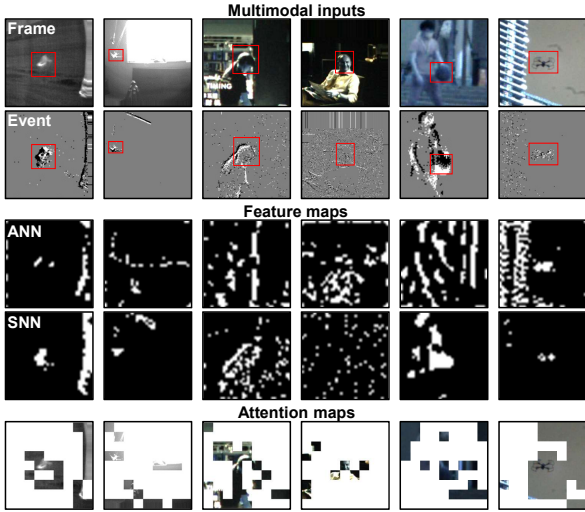


Figure 7: Visualization of the produced feature maps and attention maps. The feature maps are randomly selected from representative channels in the high-level feature F_h^i and G_h^i while the attention maps are transformed into masks and overlaid on the frame inputs to facilitate a visual interpretation. The red boxes indicate the ground truths.

modalities into a unified visual feature space, we employed an enhanced transformer-based module to effectively fuse the discriminative features across different domains. The performance of our proposed approach was evaluated on benchmark datasets, and the results demonstrated the superiority of the MMHT model over other state-of-the-art models.

In subsequent ablation experiments, we further demonstrated that the proposed fusion model can effectively integrate crucial visual cues from different visual modalities, achieving reliable object tracking across various challenging attributes. The backbones were analyzed in terms of both their effectiveness and energy consumption, thus explaining why it is necessary to use SNNs for extracting features from event modality inputs. Furthermore, in contrast with various multimodal fusion strategies, our MMHT model consistently upheld its superiority.

In future work, we will continue to refine our MMHT model to enhance its tracking performance in more intricate scenarios and improve its tracking speed. Furthermore, we will direct our attention toward addressing

challenging multi-object tracking tasks.

Acknowledgments

This work was supported in part by the STI 2030 Major Project under grant 2022ZD0208500, in part by the National Key Research and Development Program of China under grant 2023YFF1204202, in part by the National Natural Science Foundation of China under grant 82072011 and in part by Sichuan Science and Technology Program under grant 2024NSFJQ0004.

References

- [1] Bhat, G., Danelljan, M., Gool, L.V., Timofte, R., 2019. Learning discriminative model prediction for tracking, in: Proc. IEEE/CVF Int. Conf. Comput. Vis. (ICCV), pp. 6182–6191.
- [2] Brown, T., Mann, B., Ryder, N., Subbiah, M., Kaplan, J.D., Dhariwal, P., Neelakantan, A., Shyam, P., Sastry, G., Askell, A., et al., 2020. Language models are few-shot learners, in: Proc. Adv. Neural Inf. Process. Syst. (NIPS).
- [3] Cai, W., Sun, H., Liu, R., Cui, Y., Wang, J., Xia, Y., Yao, D., Guo, D., 2022. A spatial-channel-temporal-fused attention for spiking neural networks. IEEE Trans. Neural Netw. Learn. Syst. in press.
- [4] Chen, Y., Mai, Y., Feng, R., Xiao, J., 2022. An adaptive threshold mechanism for accurate and efficient deep spiking convolutional neural networks. Neurocomputing 469, 189–197.
- [5] Chen, Z., Wu, J., Hou, J., Li, L., Dong, W., Shi, G., 2023. Ecsnet: Spatio-temporal feature learning for event camera. IEEE Trans. Circuits Syst. Video Technol. 33, 701–712. doi:10.1109/TCSVT.2022.3202659.
- [6] Danelljan, M., Bhat, G., Khan, F.S., Felsberg, M., 2019. Atom: Accurate tracking by overlap maximization, in: Proc. IEEE/CVF Conf. Comput. Vis. Pattern Recognit. (CVPR), pp. 4660–4669.
- [7] Danelljan, M., Gool, L.V., Timofte, R., 2020. Probabilistic regression for visual tracking, in: Proc. IEEE/CVF Conf. Comput. Vis. Pattern Recognit. (CVPR), pp. 7183–7192.
- [8] Deng, J., Dong, W., Socher, R., Li, L.J., Li, K., Fei-Fei, L., 2009. Imagenet: A large-scale hierarchical image database, in: Proc. IEEE/CVF Conf. Comput. Vis. Pattern Recognit. (CVPR), pp. 248–255.
- [9] Dosovitskiy, A., Beyer, L., Kolesnikov, A., Weissenborn, D., Zhai, X., Unterthiner, T., Dehghani, M., Minderer, M., Heigold, G., Gelly, S., Uszkoreit, J., Houlsby, N., 2021. An image is worth 16x16 words: Transformers for image recognition at scale, in: Int. Conf. Learn. Repr. (ICLR).
- [10] El Shair, Z., Rawashdeh, S.A., 2022. High-temporal-resolution object detection and tracking using images and events. Journal of Imaging 8, 210.

- [11] Goodale, M.A., Milner, A.D., 1992. Separate visual pathways for perception and action. *Trends Neurosci.* 15, 20–25.
- [12] He, K., Zhang, X., Ren, S., Sun, J., 2016. Deep residual learning for image recognition, in: *Proc. IEEE/CVF Conf. Comput. Vis. Pattern Recognit. (CVPR)*, pp. 770–778.
- [13] Howard, A.G., Zhu, M., Chen, B., Kalenichenko, D., Wang, W., Weyand, T., Andreetto, M., Adam, H., 2017. Mobilenets: Efficient convolutional neural networks for mobile vision applications. *arXiv preprint arXiv:1704.04861*.
- [14] Hu, J., Shen, L., Sun, G., 2018. Squeeze-and-excitation networks, in: *Proceedings of the IEEE conference on computer vision and pattern recognition*, pp. 7132–7141.
- [15] Hu, Q., Meng, L., Liu, Y., Hu, S., Qiao, G., 2023. Siamese network object tracking based on fusion of visible and event cameras, in: *Proc. Int. Conf. Cyb. Secur. Artif. Intell. Digi. Econ. (CSAIDE)*, p. 127181R.
- [16] Hui, T., Xun, Z., Peng, F., Huang, J., Wei, X., Wei, X., Dai, J., Han, J., Liu, S., 2023. Bridging search region interaction with template for rgb-t tracking, in: *Proc. IEEE/CVF Conf. Comput. Vis. Pattern Recognit. (CVPR)*, pp. 13630–13639.
- [17] Ji, M., Wang, Z., Yan, R., Liu, Q., Xu, S., Tang, H., 2023. Sctn: Event-based object tracking with energy-efficient deep convolutional spiking neural networks. *Frontiers in Neuroscience* 17, 1123698.
- [18] Jiang, R., Han, J., Xue, Y., Wang, P., Tang, H., 2023. Cmc: A robust multimodal fusion method for spiking neural networks, in: *Proc. Int. Conf. Neural Inf. Processing (ICNIP)*, pp. 159–171.
- [19] Kingma, D.P., Ba, J., 2014. Adam: A method for stochastic optimization. *arXiv:1412.6980*.
- [20] Krizhevsky, A., Sutskever, I., Hon, G.E., 2012. Imagenet classification with deep convolutional neural networks, in: *Proc. Adv. Neural Inf. Process. Syst. (NIPS)*.
- [21] Li, H., Liu, H., Ji, X., Li, G., Shi, L., 2017. Cifar10-dvs: An event-stream dataset for object classification. *Front. Neurosci.* 11, 309.
- [22] Li, J., Dong, S., Yu, Z., Tian, Y., Huang, T., 2019. Event-based vision enhanced: A joint detection framework in autonomous driving, in: *2019 IEEE International Conference on Multimedia and Expo (ICME)*, IEEE. pp. 1396–1401.
- [23] Li, S., Gao, J., Li, L., Wang, G., Wang, Y., Yang, X., 2022. Dual-branch approach for tracking uavs with the infrared and inverted infrared image, in: *Proc. Int. Conf. Intell. Comput. Sign. Process (ICSP)*, IEEE. pp. 1803–1806.
- [24] Liu, S., Liu, D., Srivastava, G., Połap, D., Woźniak, M., 2021. Overview and methods of correlation filter algorithms in object tracking. *Complex. Intell. Syst.* 7, 1895–1917.
- [25] Luo, W., Xing, J., Milan, A., Zhang, X., Liu, W., Kim, T.K., 2021. Multiple object tracking: A literature review. *Artif. Intell.* 293, 103448.
- [26] Ma, C., Yan, R., Yu, Z., Yu, Q., 2022. Deep spike learning with local classifiers. *IEEE Trans. Cyber.* 53, 3363–3375.
- [27] Maass, W., 1997. Networks of spiking neurons: the third generation of neural network models. *Neural Netw.* 10, 1659–1671.
- [28] Messikommer, N., Fang, C., Gehrig, M., Scaramuzza, D., 2023. Data-driven feature tracking for event cameras, in: *Proc. IEEE/CVF Conf. Comput. Vis. Pattern Recognit. (CVPR)*, pp. 5642–5651.
- [29] Pei, J., Deng, L., Song, S., Zhao, M., Zhang, Y., Wu, S., Wang, G., Zou, Z., Wu, Z., He, W., et al., 2019. Towards artificial general intelligence with hybrid tianjic chip architecture. *Nature* 572, 106–111.
- [30] Qu, J., Gao, Z., Zhang, T., Lu, Y., Tang, H., Qiao, H., 2023. Spiking neural network for ultra-low-latency and high-accurate object detection. *arXiv:2306.12010*.
- [31] Ren, S., He, K., Girshick, R., Sun, J., 2015. Faster r-cnn: Towards real-time object detection with region proposal networks, in: *Proc. Adv. Neural Inf. Process. Syst. (NIPS)*, Curran Associates, Inc.
- [32] Song, S., Ma, C., Sun, W., Xu, J., Dang, J., Yu, Q., 2021. Efficient learning with augmented spikes: A case study with image classification. *Neural Networks* 142, 205–212.
- [33] Sun, H., Cai, W., Yang, B., Cui, Y., Xia, Y., Yao, D., Guo, D., 2023. A synapse-threshold synergistic learning approach for spiking neural networks. *IEEE Trans. Cogn. Dev. Syst.* in press.
- [34] Tang, C., Wang, X., Huang, J., Jiang, B., Zhu, L., Zhang, J., Wang, Y., Tian, Y., 2022. Revisiting color-event based tracking: A unified network, dataset, and metric. *arXiv:2211.11010*.
- [35] Vaswani, A., Shazeer, N., Parmar, N., Uszkoreit, J., Jones, L., Gomez, A.N., Kaiser, Ł., Polosukhin, I., 2017. Attention is all you need, in: *Proc. Adv. Neural Inf. Process. Syst. (NIPS)*.
- [36] Wang, X., Li, J., Zhu, L., Zhang, Z., Chen, Z., Li, X., Wang, Y., Tian, Y., Wu, F., 2021. Visevent: Reliable object tracking via collaboration of frame and event flows. *arXiv:2108.05015*.
- [37] Wang, X., Wu, Z., Rong, Y., Zhu, L., Jiang, B., Tang, J., Tian, Y., 2023. Sstformer: Bridging spiking neural network and memory support transformer for frame-event based recognition. *arXiv:2308.04369*.
- [38] Wu, Y., Deng, L., Li, G., Zhu, J., Shi, L., 2018. Spatio-temporal backpropagation for training high-performance spiking neural networks. *Front. Neurosci.* 12, 331.
- [39] Wu, Y., Deng, L., Li, G., Zhu, J., Xie, Y., Shi, L., 2019. Direct training for spiking neural networks: Faster, larger, better, in: *Proc. AAAI Conf. Artif. Intell. (AAAI)*, pp. 1311–1318.
- [40] Wu, Z., Zheng, J., Ren, X., Vasluianu, F.A., Ma, C., Paudel, D.P., Van Gool, L., Timofte, R., 2023. Single-model and any-modality for video object tracking. *arXiv preprint arXiv:2311.15851*.
- [41] Xiao, Y., Yang, M., Li, C., Liu, L., Tang, J., 2022. Attribute-based progressive fusion network for rgbt tracking, in: *Proc. AAAI Conf. Artif. Intell. (AAAI)*, pp. 2831–2838.
- [42] Yang, J., Gao, S., Li, Z., Zheng, F., Leonardis, A., 2023a. Resource-efficient rgbd aerial tracking, in: *Proc. IEEE/CVF Conf. Comput. Vis. Pattern Recognit. (CVPR)*, pp. 13374–13383.
- [43] Yang, J., Li, Z., Zheng, F., Leonardis, A., Song, J., 2022. Prompting for multi-modal tracking, in: *Proc. ACM Int. Conf. Multimedia (ACM MM)*, pp. 3492–3500.
- [44] Yang, Y., Pan, L., Liu, L., 2023b. Event camera data pre-training. *arXiv:2301.01928*.
- [45] Yang, Z., Wu, Y., Wang, G., Yang, Y., Li, G., Deng, L., Zhu, J., Shi, L., 2019. Dashnet: A hybrid artificial and spiking neural network for high-speed object tracking. *arXiv:1909.12942*.
- [46] Yao, M., Zhang, H., Zhao, G., Zhang, X., Wang, D., Cao, G., Li, G., 2023a. Sparser spiking activity can be better: Feature refine-and-mask spiking neural network for event-based visual recognition. *Neural Netw.* 166, 410–423.
- [47] Yao, M., Zhao, G., Zhang, H., Hu, Y., Deng, L., Tian, Y., Xu, B., Li, G., 2023b. Attention spiking neural networks. *IEEE Trans. Pattern Anal. Mach. Intell.* 45, 9393–9410. doi:10.1109/TPAMI.2023.3241201.
- [48] Ye, B., Chang, H., Ma, B., Shan, S., Chen, X., 2022. Joint feature learning and relation modeling for tracking: A one-stream framework, in: *Proc. Eur. Conf. Comput. Vis. (ECCV)*, Springer. pp. 341–357.
- [49] Yu, F., Wu, Y., Ma, S., Xu, M., Li, H., Qu, H., Song, C., Wang, T., Zhao, R., Shi, L., 2023. Brain-inspired multimodal hybrid neural network for robot place recognition. *Sci. Robot.* 8, eabm6996.
- [50] Zeng, Z., Li, X., Fan, C., Zou, L., Chi, R., 2023. Swineft: a

- robust and powerful swin transformer based event frame tracker. *Applied Intelligence*, 1–18.
- [51] Zhang, J., Dong, B., Zhang, H., Ding, J., Heide, F., Yin, B., Yang, X., 2022. Spiking transformers for event-based single object tracking, in: *Proc. IEEE/CVF Conf. Comput. Vis. Pattern Recognit. (CVPR)*, pp. 8801–8810.
- [52] Zhang, J., Wang, Y., Liu, W., Li, M., Bai, J., Yin, B., Yang, X., 2023a. Frame-event alignment and fusion network for high frame rate tracking, in: *Proc. IEEE/CVF Conf. Comput. Vis. Pattern Recognit. (CVPR)*, pp. 9781–9790.
- [53] Zhang, J., Yang, X., Fu, Y., Wei, X., Yin, B., Dong, B., 2021. Object tracking by jointly exploiting frame and event domain, in: *Proc. IEEE/CVF Int. Conf. Comput. Vis. (ICCV)*, pp. 13043–13052.
- [54] Zhang, T., Guo, H., Jiao, Q., Zhang, Q., Han, J., 2023b. Efficient rgb-t tracking via cross-modality distillation, in: *Proc. IEEE/CVF Conf. Comput. Vis. Pattern Recognit. (CVPR)*, pp. 5404–5413.
- [55] Zhao, R., Yang, Z., Zheng, H., Wu, Y., Liu, F., Wu, Z., Li, L., Chen, F., Song, S., Zhu, J., et al., 2022. A framework for the general design and computation of hybrid neural networks. *Nat. Commun.* 13, 3427.
- [56] Zhu, A.Z., Thakur, D., Özaslan, T., Pfrommer, B., Kumar, V., Daniilidis, K., 2018. The multivehicle stereo event camera dataset: An event camera dataset for 3d perception. *IEEE Robot. Autom. Lett.* 3, 2032–2039.
- [57] Zhu, J., Lai, S., Chen, X., Wang, D., Lu, H., 2023a. Visual prompt multi-modal tracking, in: *Proc. IEEE/CVF Conf. Comput. Vis. Pattern Recognit. (CVPR)*, pp. 9516–9526.
- [58] Zhu, Z., Hou, J., Wu, D.O., 2023b. Cross-modal orthogonal high-rank augmentation for rgb-event transformer-trackers, in: *Proc. IEEE/CVF Int. Conf. Comput. Vis. (ICCV)*, pp. 22045–22055.